A NOVEL HOLLOW-GLASS MICROSPHERE SENSOR FOR MONITORING HIGH HYDROSTATIC PRESSURE

M. G. Xu and J. P. Dakin

Optoelectronics Research Centre
University of Southampton
Southampton SO9 5NH
U.K.

ABSTRACT

Laboratory prototypes of a novel pressure sensor have been produced using a hollow glass microsphere, bonded, in an on-axis position, to the end of a monomode optical fibre. The sphere surfaces form a low finesse Fabry-Perot interferometer. The construction of the probe is simple in concept, yet the sensing element is intrinsically hermetically sealed. Experimental trials, under the influence of hydraulic pressure have been carried out and show a good match with predicted behaviour. The observed shift in wavelength with pressure was -0.93 nm/MPa, two orders of magnitude higher than that we have measured with a in-fibre-grating sensor under similar conditions. The ratio of the pressure sensitivity to the temperature sensitivity for our microsphere sensor was more than two orders of magnitude better than the in-fibre-grating type, so therefore less compensation is necessary to correct for temperature changes. This new form of sensing probe has potential for many high-pressure sensing applications.

1. INTRODUCTION

Fabry-Perot (F-P) sensors have been reported for the measurement of strain, temperature, pressure, vibration and acoustic waves[1,2]. Several methods of creating extrinsic fibre-optic F-P interferometers have been described[3-5]. Fairly sophisticated separation methods are required in the probe head to maintain the mirror spacing, yet allow the sensor to be sealed against ingress of foreign material. In our method a hollow glass microsphere is bonded, in an on-axis position, to the end of a monomode optical fibre. A low finesse F-P cavity is then formed between the sphere surfaces. The main advantages of our new arrangement is that the probe is simple, miniature and hermetically sealed. As with earlier F-P sensors[3-5], the probe is conveniently addressed by monitoring its reflection spectrum. The wavelength of each peak reflection and the span between peaks are both dependent on the physical spacing between the reflective surfaces.

2. SENSOR CONSTRUCTION

A schematic of the sensor construction is shown in Fig.1. Light from a 1550 nm fibre-pigtailed ELED is coupled into the sensor head via a directional fibre coupler. The sensing probe was tested within a cavity in a high pressure vessel, hydraulic pressure being applied to compress the sphere. The reflectance of the probe was monitored using a commercial optical spectrum analyser (ANDO AQ-6310B), located to receive light from a return port of the coupler. Reflections from the unused output port of the coupler were suppressed using index-matching oil. The hydraulic pressure system consisted of a hydraulic pump, a commercial precision pressure transmitter (Druck PDCR 960) and a purpose-designed pressure vessel capable of being used up to 70 MPa.

3. THEORY OF THE F-P SENSOR

The observed F-P interference occurs between light reflected from the spherical surfaces of the glass bubble sensing element. Only the first reflections from each inner surface of the sphere were significant in our sensor as, firstly, the reflection was low at each surface and, secondly, the outer surfaces of the sphere were matched by bonding cement. As a result, the interference can be considered to be essentially two-wave interference only. The observed intensity, I_D, at the optical spectrum analyser is then a result of coherent superposition of light arising from reflections at each inner surface of the hollow glass sphere. I_D is given by:

$$I_D = k[A_1^2 + A_2^2 + 2A_1A_2\cos(\frac{2\pi}{\lambda}2d)] \quad (1)$$

where k is a constant, A_1 and A_2 represent the electric field amplitudes of the interfering light from the two surfaces of the sphere, λ is the wavelength of the source, and d is the spacing within the F-P cavity (ie. d is the inner diameter of the sphere). The free spectral range (FSR) of the F-P resonant cavity is given by:

$$FSR = \frac{c}{2d} \quad (2)$$

Where c is the free-space velocity of the light. Maxima in the reflectance spectrum occur when:

$$\lambda = \frac{2d}{m} \quad (3)$$

where m is an integer. By differentiating equation (3), and substituting for m, the change in wavelength of peak reflection, $\Delta\lambda$, resulting from a change in pressure, ΔP, is given by:

$$\Delta\lambda = \frac{\lambda}{d}\frac{\delta d}{\delta P}\Delta P \quad (4)$$

The effect of isotropic pressure on a perfect hollow sphere would normally be to cause only a compressive load on the material and reduce its diameter. A perfect sphere should therefore be capable of withstanding enormous pressure. In practice, however, an imperfect sphere, or one which is bonded to an external body on one side, as ours was, will suffer asymmetrical compression and will hence collapse at high pressure. We shall assume, for the present, in our analysis, that the sphere is perfect and that the pressure is isotropically applied. The induced strain, Δd, in a hollow sphere, exposed to a isotropic external pressure, P, can be expressed as[6]:

$$\Delta d = -\frac{Pd^2(1-\nu)}{4Yt} \quad (5)$$

where t is the wall thickness of the sphere, and Y and ν are the Young's modulus and Poisson's ratio of the material of the sphere, respectively. From eqn. (4) and (5), we obtain the response of the sensor in terms of the pressure-induced fringe shift:

$$\Delta\lambda = -\frac{\lambda d(1-\nu)}{4Yt}\Delta P \qquad (6)$$

This relationship shows that, as expected, the sensitivity to pressure can be increased by choosing a larger diameter sphere, provided the wall thickness remains the same. The most suitable wavelength to choose for monitoring of the fringe-shift will depend on the spectral response of the source. The expected cross-sensitivity to a change in temperature, ΔT, is given by:

$$\Delta\lambda = \frac{\lambda}{d}\frac{\delta d}{\delta T}\Delta T \qquad (7)$$

4. RESULTS AND DISCUSSION

Figure 2 shows the reflected spectrum, observed in the wavelength domain, with a sensing probe fitted with a 120 μm diameter sphere of approximately 0.8μm wall thickness. This spectrum shows a fringe spacing of 10 nm, as expected from eqn. (2). The maximum intensity contrast of the fringes between peaks and minima of the reflected spectrum was 3.8 dB. The pressure response of the sensor is shown in Fig. 3. This shows the variation of the wavelength of a particular reflection maximum (chosen to be 1552.47 nm at zero pressure) with pressure. The mechanical compliance of a hollow sphere is much higher than that of a solid body, such as a fibre or an in-fibre grating, so the fractional shift in wavelength with pressure is naturally much higher. From eqn.(6), we would have expected a pressure response of -0.83 nm/MPa, whereas our measured gradient was -0.93 nm/MPa. Uncertainties in the wall thickness of the sphere and our lack of knowledge of the precise value for Young's modulus for the material of our sphere are the most likely reason for the discrepancy.

The hollow-glass spheres used in our experiment are made from C-glass (soda-lime-borosilicate). We were unfortunately unable to obtain precise information on the material used, so we have assumed a typical Young's modulus value of 7×10^{10} N/m^2 and a Poisson's ratio value of 0.2, typical for C-glass, in order to perform our sensitivity calculation. As we mentioned earlier, a perfect sphere should withstand enormous isotropic pressure. Our sphere is bonded on one side to the optical fibre, so we expected it to implode eventually. In our first trials we deliberately tested the sensor up to the implosion point. The observed implosion pressure for spheres in our experiment was typically above 7 MPa. This should be adequate for many applications. For higher pressure measurement, a smaller or thicker-walled sphere could be used. A particular advantage of this new sensor is that the wavelength shift observed in our experiment was two orders of magnitude higher than that we have recently measured with a in-fibre-grating pressure sensor[7]. Of course, the pressure sensitivity could be increased further by choosing a larger sphere of the same wall thickness, but this would be likely to lead to a lower implosion limit.

Measurements of the cross-sensitivity to temperature of our sensing probe, shown in Fig.4, indicate that the errors due to temperature changes are relatively small. The measured temperature coefficient of wavelength variation was 0.0077 nm/°C. In particular, the ratio of the responses of the glass bubble to pressure and temperature were over two orders of magnitude better than we observed for the in-fibre-grating sensor.

5. CONCLUSIONS

A novel fibre optic sensor for monitoring hydrostatic pressure has been constructed. The sensor head is extremely small, the construction is simple and the sensing element has intrinsic hermetic sealing. A fringe displacement of 5.8 nm at 6.3 MPa pressure was observed. The sensitivity is two orders of magnitude higher than we have measured with a in-fibre-grating pressure sensor, and the relative effects of cross-sensitivity to temperature are much less.

6. ACKNOWLEDGMENT

The authors wish to thank Dr G. Wylangowski for assistance with the design and test of the pressure vessel and for providing glass capillaries for the sensor construction.

7. REFERENCES

1. Toshihiko Yoshino et al, "Fiber-optic Fabry-Perot Interferomter and its Sensor Applications", IEEE. J. of Quantum Electronics, Vol.QE-18, No.10,1624 (1982)

2. Gordon. L. Mitchell, "A Review of Fabry-Perot Interferometric Sensors", Springer Proc. in Physics, Vol.44, 450(1989)

3. Paul J. Kuzmenko, "Experimental Performance of A Miniature Fabry-Perot Fibre Optic Hydrophone", Proc. OFS, 354(1992)

4. Kent A. Murphy et al, "Extrinsic Fabry-Perot Optical Fibre Sensor", ibid, p193.

5. Lee. C. E. et al, "Metal-embedded fibre-optic Fabry-Perot sensors", Optics Lett. Vol.16, No.24 1990(1991)

6. Raymond J. Roark, Warren C. Young, "Formulas for Stress and Strain" (5th Edition), McGraw-Hill International Book Company, p451.

7. Ming. G. Xu and John. P. Dakin, "Optical Fibre Sensor for High Pressure Measurement Using an in-Fibre-Grating", to be submitted for publication.

A NOVEL HOLLOW-GLASS MICROSPHERE SENSOR FOR MONITORING HIGH HYDROSTATIC PRESSURE

M. G. Xu and J. P. Dakin

Optoelectronics Research Centre
University of Southampton
Southampton SO9 5NH
United Kingdom

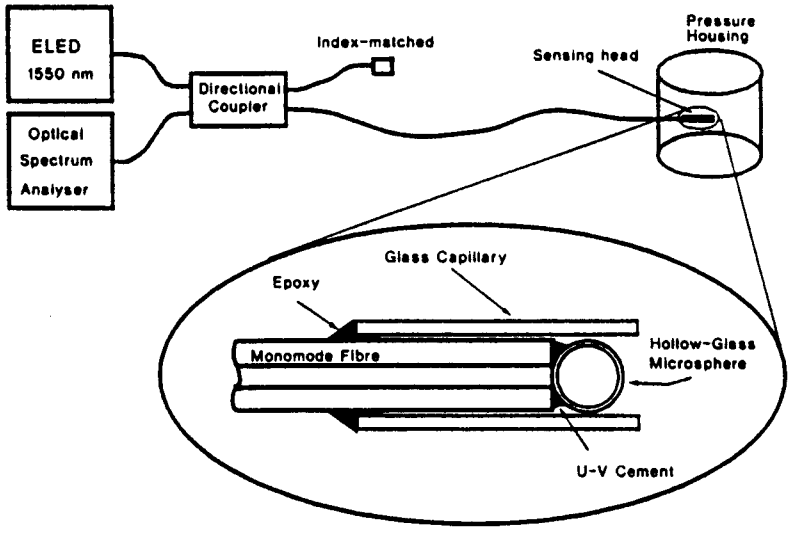

Fig 1. Schematic of the hollow-glass microsphere pressure sensor

Reflected spectrum from microsphere with LED excitation

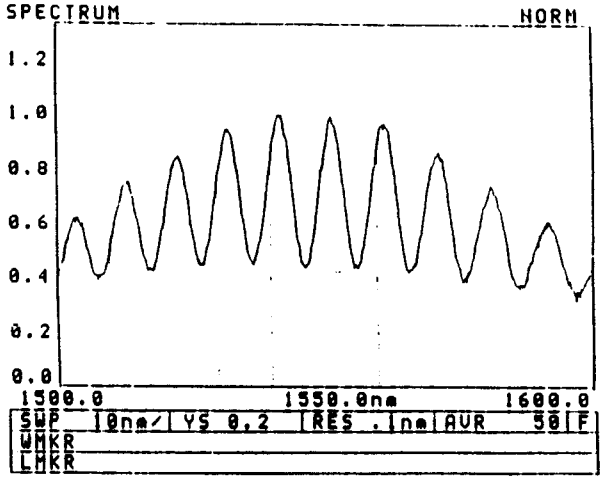

Pressure response of the sensor

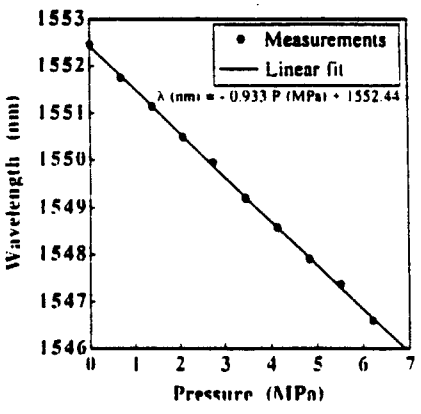

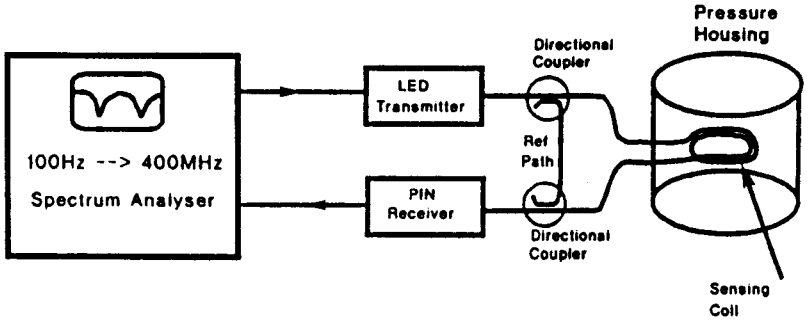

Fig 1. Schematic of Experimental Pressure Sensing Arrangement

Thermal response of the sensor (ie. Temperature cross-sensitivity)

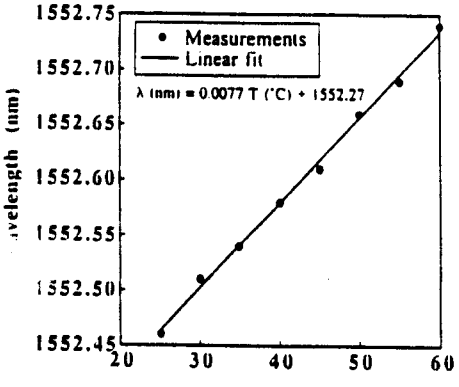

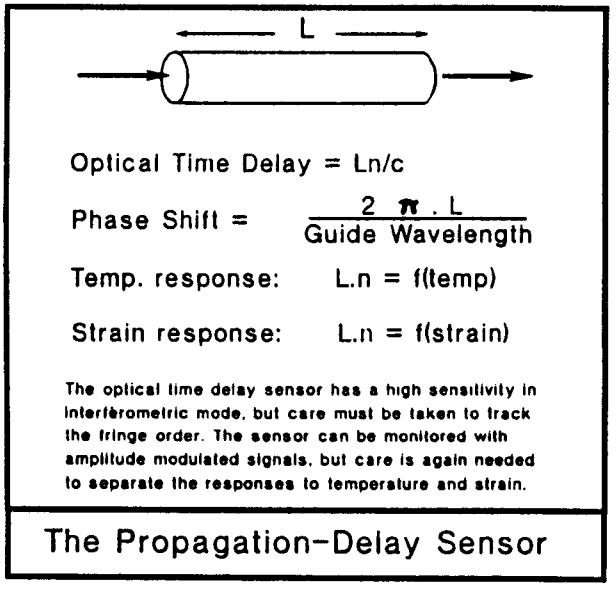

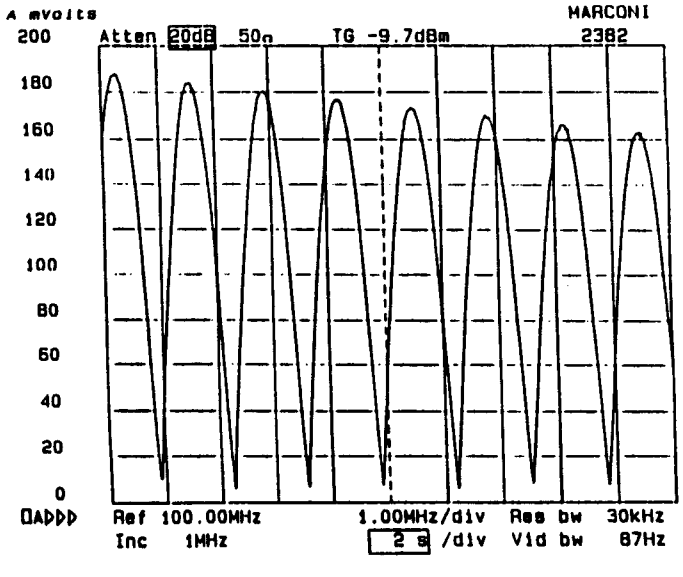

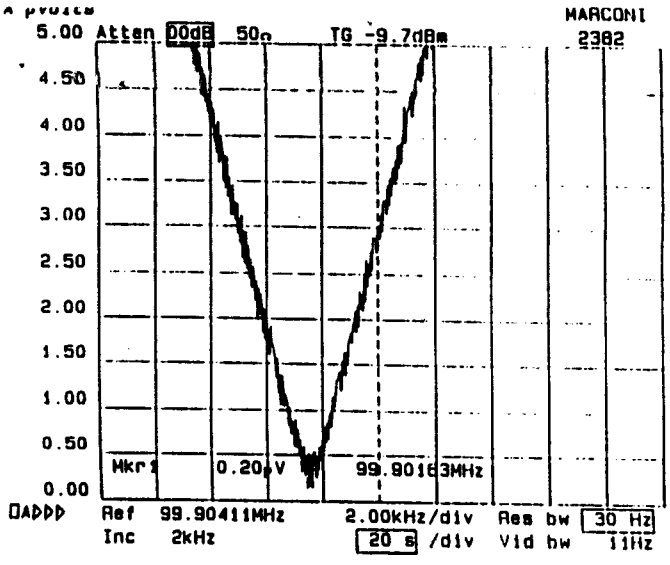

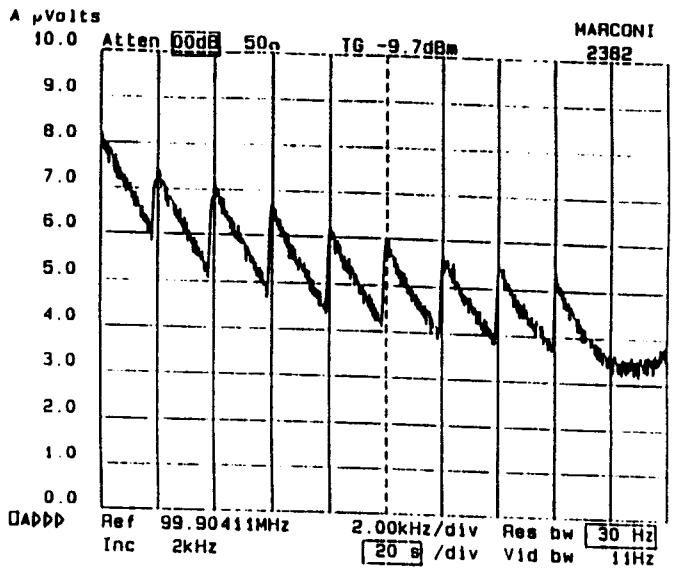

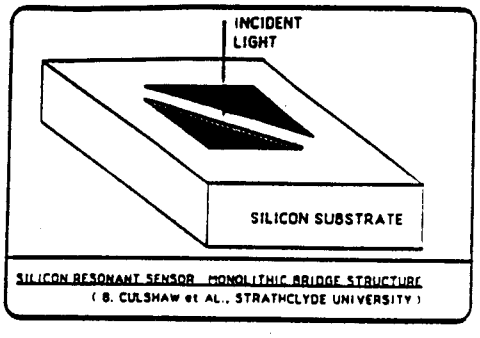

SILICON RESONANT SENSOR MONOLITHIC BRIDGE STRUCTURE
(B. CULSHAW et AL., STRATHCLYDE UNIVERSITY)

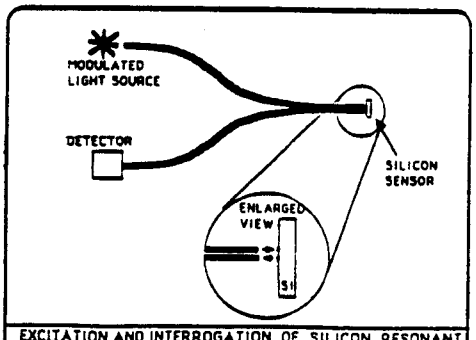

EXCITATION AND INTERROGATION OF SILICON RESONANT SENSOR USING TWIN FIBRE LEADS.

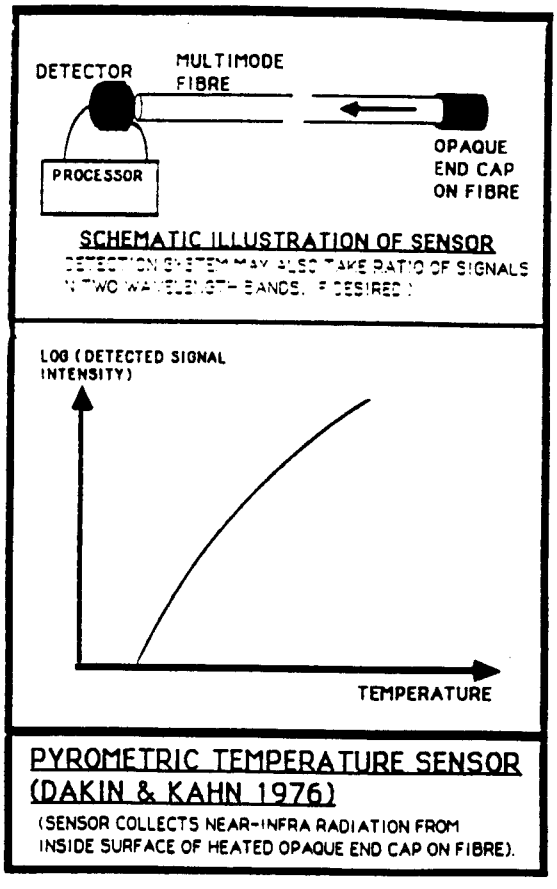

PYROMETRIC TEMPERATURE SENSOR (DAKIN & KAHN 1976)

(SENSOR COLLECTS NEAR-INFRA RADIATION FROM INSIDE SURFACE OF HEATED OPAQUE END CAP ON FIBRE).

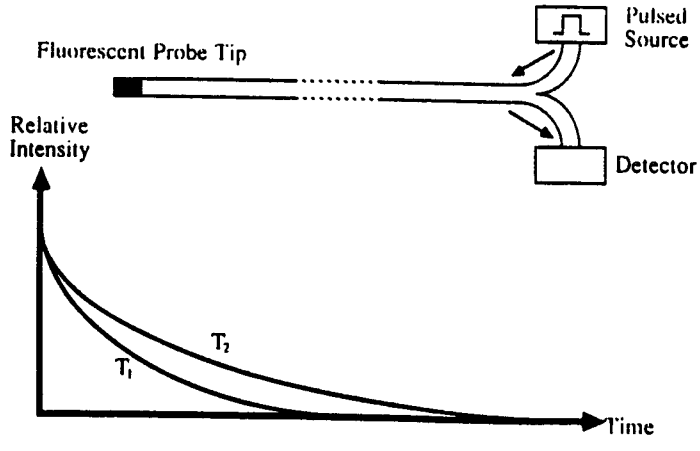

FLUORESCENT DECAY TIME SENSOR (Cormack)

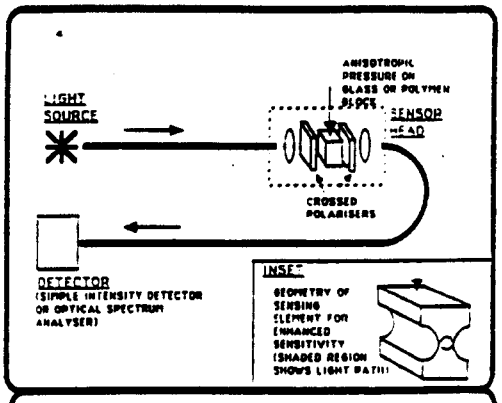

SCHEMATIC ILLUSTRATION OF PHOTO-ELASTIC PRESSURE SENSOR.(SPILLMAN & Mc. MAHON) (SPECTRAL INTERROGATION VERSION BY SPOONCER)

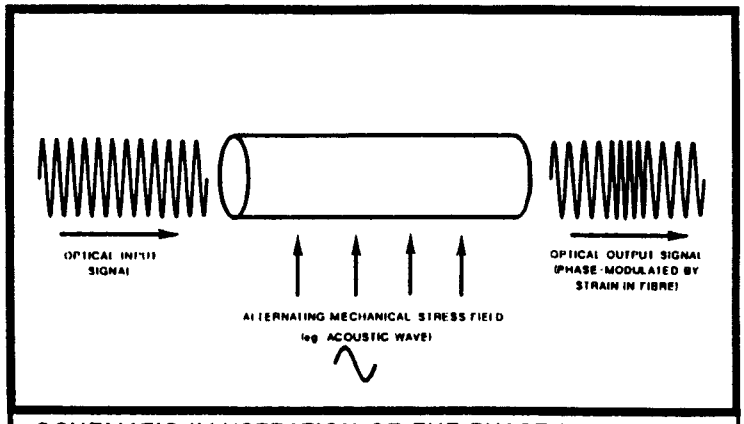

SCHEMATIC ILLUSTRATION OF THE PHASE MODULATION OF LIGHT BY AN ACOUSTIC WAVE ACTING ON A FIBRE.

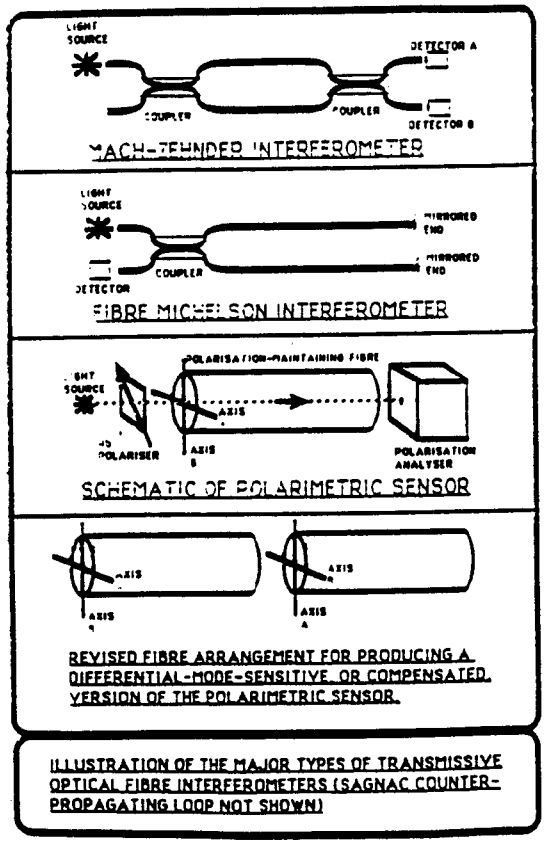

ILLUSTRATION OF THE MAJOR TYPES OF TRANSMISSIVE OPTICAL FIBRE INTERFEROMETERS (SAGNAC COUNTER-PROPAGATING LOOP NOT SHOWN)

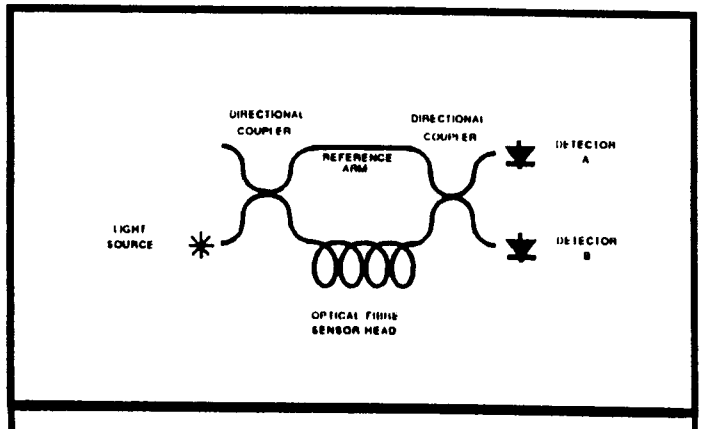

SCHEMATIC OF MACH-ZEHNDER INTERFEROMETER FOR SENSING OF ACOUSTIC SIGNALS (UNBALANCED PATH VERSION)

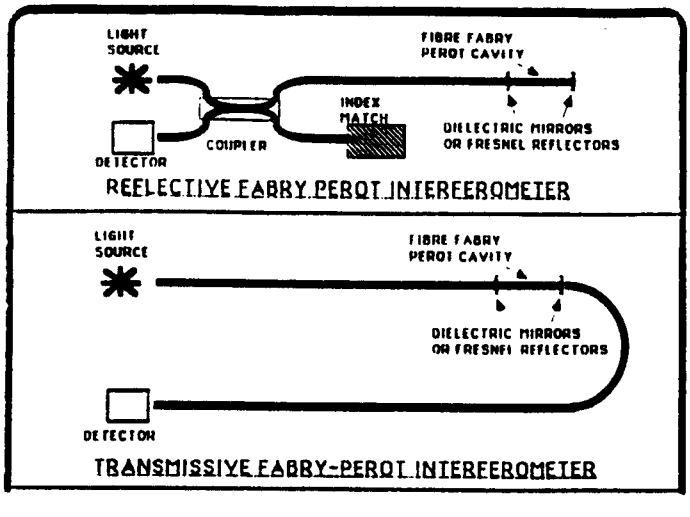

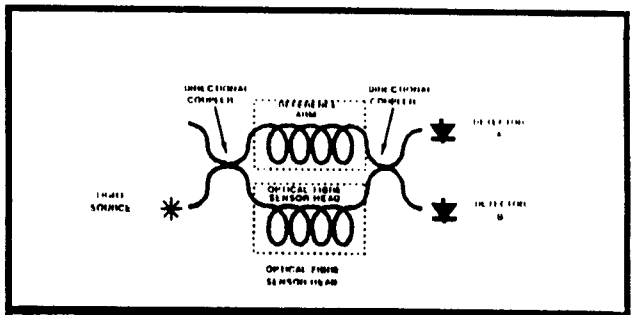

SCHEMATIC OF MACH-ZEHNDER INTERFEROMETER FOR SENSING OF ACOUSTIC SIGNALS

(BALANCED PATH VERSION, FOR DIFFERENTIAL SENSING)

NOTE THAT THE SENSOR WILL SENCE PRESSURE GRADIENT UNLESS ONE COIL IS SHIELDED FROM ACOUSTIC SIGNALS BECAUSE OF WELL-BALANCED CONFIGURATION, SOURCE PHASE NOISE IS NOT A PROBLEM AND SHORT COHERENCE LENGTH SOURCES ARE PERMITTED.

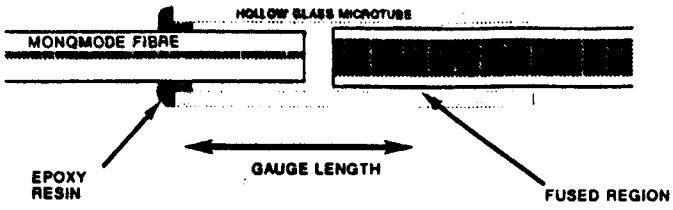

FIBRE SENSOR OF CLAUS et Al, VIRGINIA TECH, USA.

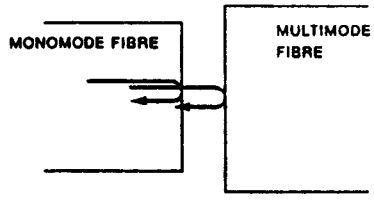

SCHEMATIC OF INTERFERING LIGHT BEAMS REFLECTED FROM EACH FIBRE END SURFACE.

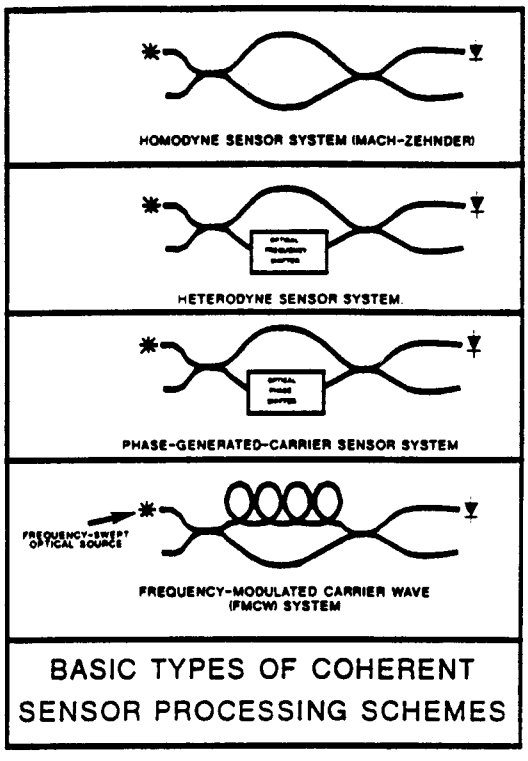

BASIC TYPES OF COHERENT SENSOR PROCESSING SCHEMES

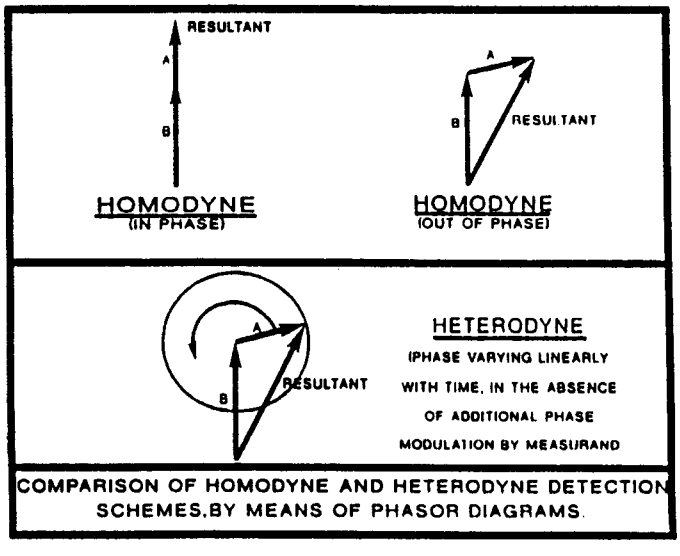

COMPARISON OF HOMODYNE AND HETERODYNE DETECTION SCHEMES, BY MEANS OF PHASOR DIAGRAMS.

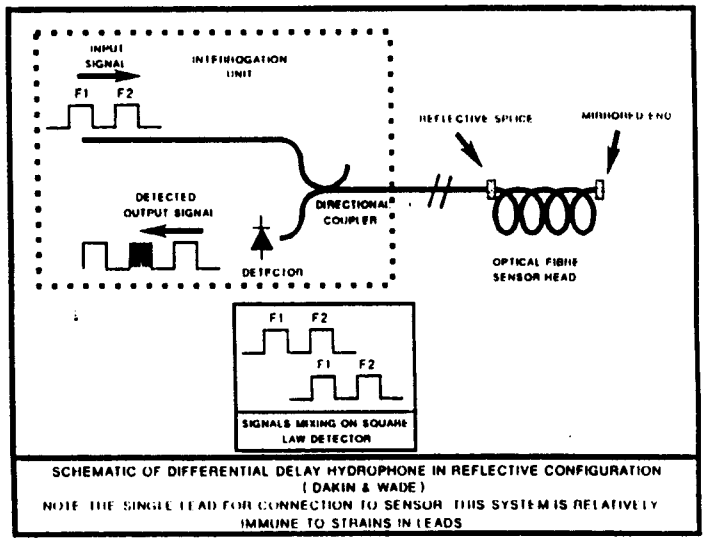

SCHEMATIC OF DIFFERENTIAL DELAY HYDROPHONE IN REFLECTIVE CONFIGURATION (DAKIN & WADE)
NOTE THE SINGLE LEAD FOR CONNECTION TO SENSOR. THIS SYSTEM IS RELATIVELY IMMUNE TO STRAINS IN LEADS

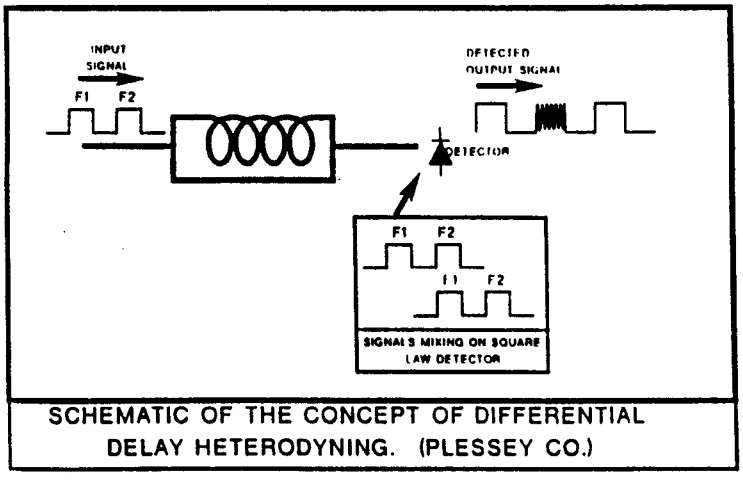

SCHEMATIC OF THE CONCEPT OF DIFFERENTIAL DELAY HETERODYNING. (PLESSEY CO.)

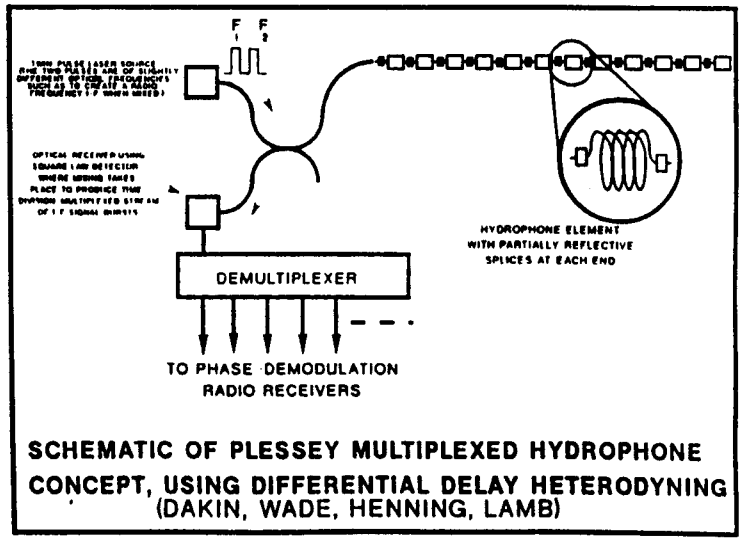

SCHEMATIC OF PLESSEY MULTIPLEXED HYDROPHONE CONCEPT, USING DIFFERENTIAL DELAY HETERODYNING (DAKIN, WADE, HENNING, LAMB)

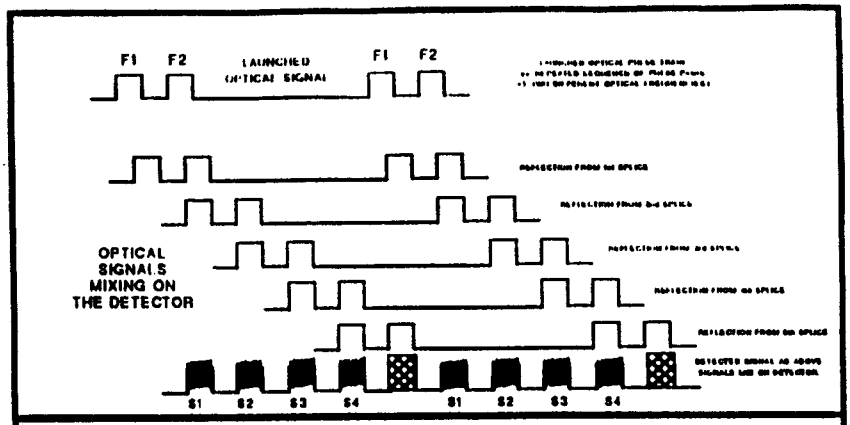

TIMING DIAGRAM OF SIGNALS FROM A 4-ELEMENT HYDROPHONE ARRAY, AS IN PREVIOUS DIAGRAM. (SYSTEM OF DAKIN AND WADE, FORMERLY OF PLESSEY Co. Ltd)

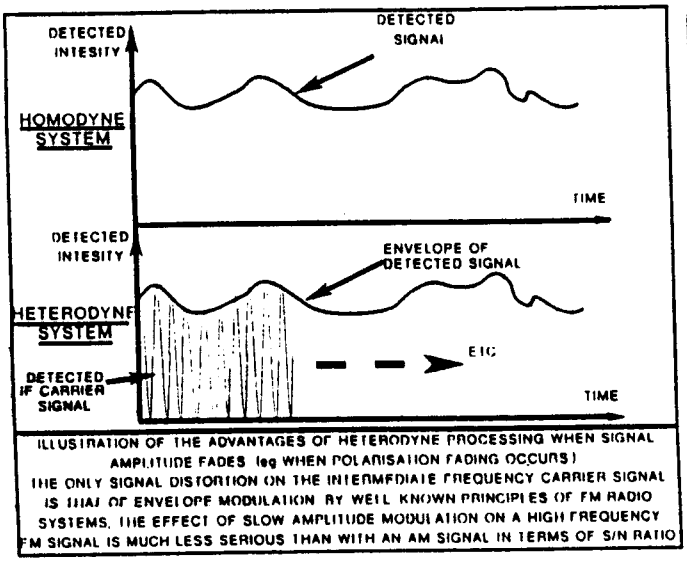

ILLUSTRATION OF THE ADVANTAGES OF HETERODYNE PROCESSING WHEN SIGNAL AMPLITUDE FADES (eg WHEN POLARISATION FADING OCCURS) THE ONLY SIGNAL DISTORTION ON THE INTERMEDIATE FREQUENCY CARRIER SIGNAL IS THAT OF ENVELOPE MODULATION BY WELL KNOWN PRINCIPLES OF FM RADIO SYSTEMS. THE EFFECT OF SLOW AMPLITUDE MODULATION ON A HIGH FREQUENCY FM SIGNAL IS MUCH LESS SERIOUS THAN WITH AN AM SIGNAL IN TERMS OF S/N RATIO

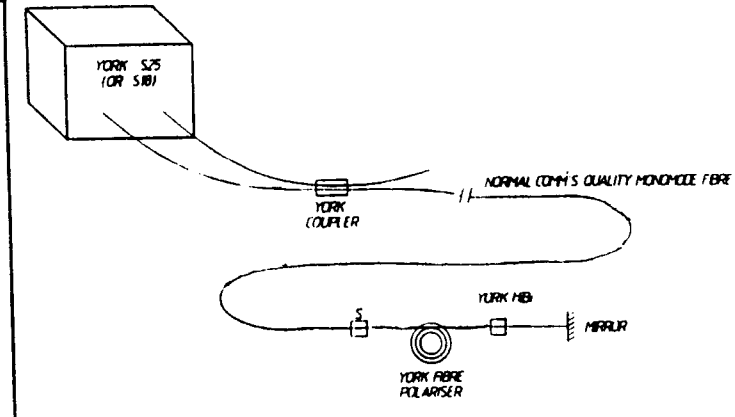

SCHEMATIC OF EXPERIMENTAL SYSTEM

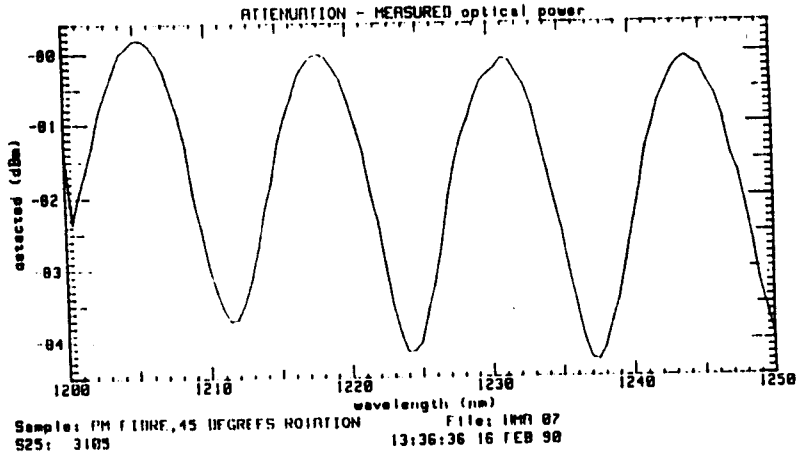

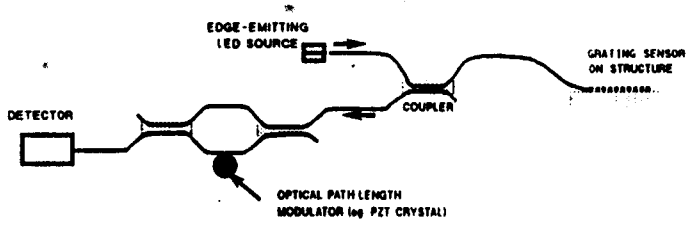

SYSTEM FOR THE INTERROGATION OF GRATING WAVELENGTH, USING INTERFEROMETER

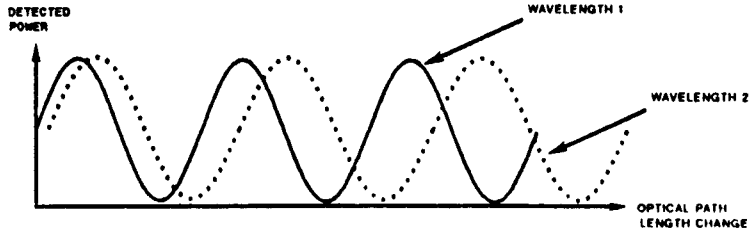

RESPONSE OF SYSTEM SHOWN IN ABOVE DIAGRAM, AS GRATING WAVELENGTH CHANGES

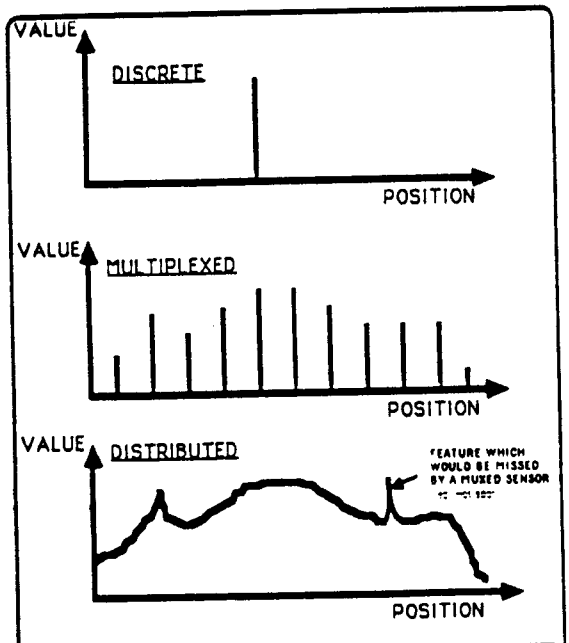

ADVANTAGES OF MULTIPLEXED AND DISTRIBUTED OPERATION

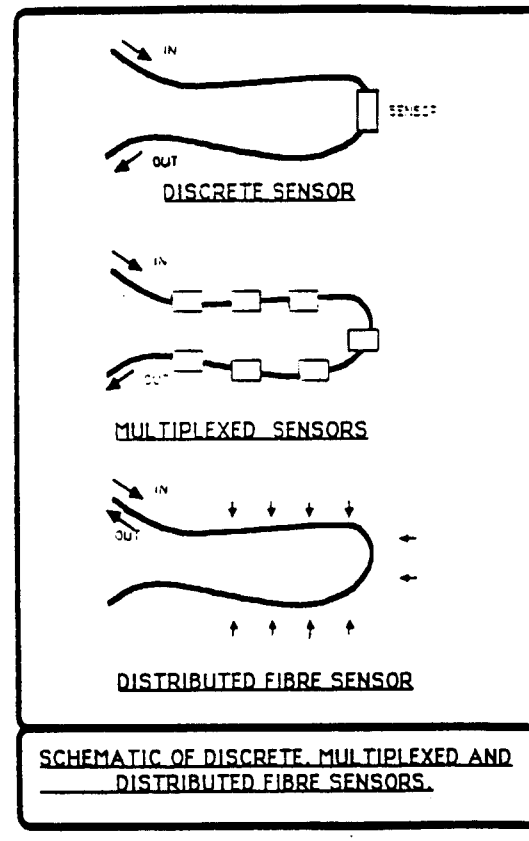

SCHEMATIC OF DISCRETE, MULTIPLEXED AND DISTRIBUTED FIBRE SENSORS.

ADVANTAGES OF DISTRIBUTED FIBRE SENSORS

- INTRINSICALLY MULTIPLEXED, WITHOUT 'GAPS' IN COVERAGE
- MORE ECONOMIC USE OF EXPENSIVE OPTOELECTRONICS
- RELIABLE COMPARISON OF MEASURAND VALUE vs LENGTH
- INOBTRUSIVE SENSOR WITH LESS CABLING

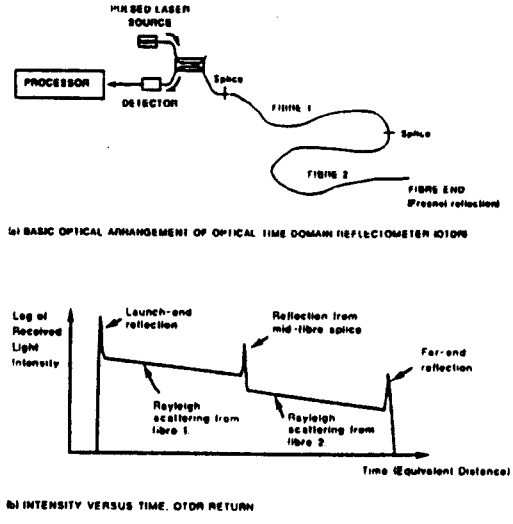

FIG 1. CONCEPT OF THE BASIC OPTICAL TIME DOMAIN REFLECTOMETER

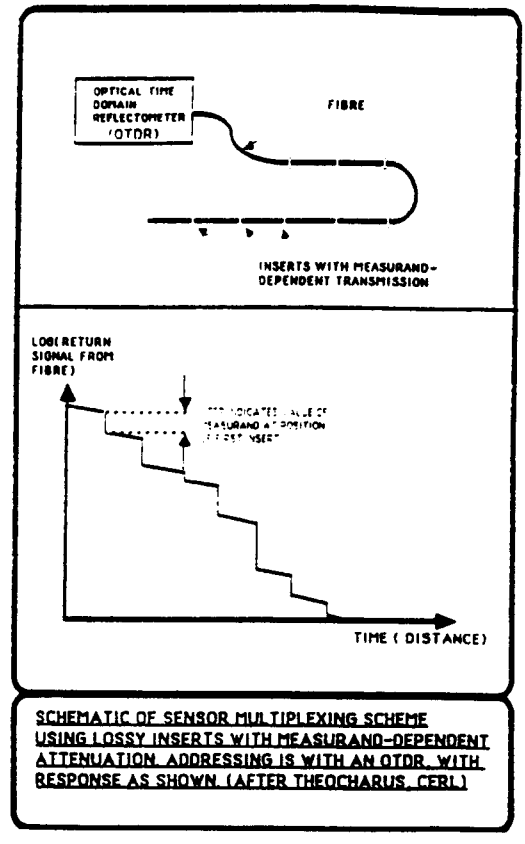

SCHEMATIC OF SENSOR MULTIPLEXING SCHEME USING LOSSY INSERTS WITH MEASURAND-DEPENDENT ATTENUATION. ADDRESSING IS WITH AN OTDR, WITH RESPONSE AS SHOWN. (AFTER THEOCHARUS, CERL)

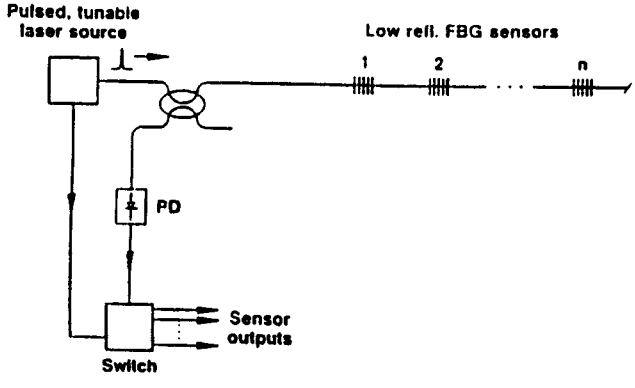

Fig. 8. Time division multiplexing of fiber grating sensors using a tunable narrowband source.

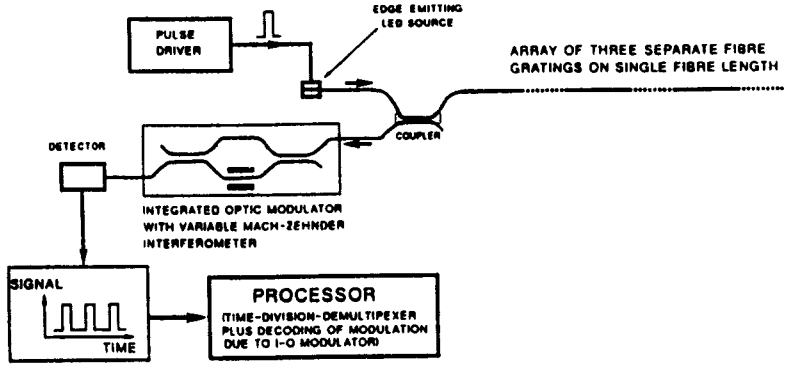

TIME-DIVISION MULTIPLEXED SYSTEM FOR THE INTERROGATION OF GRATING WAVELENGTH

(Method proposed by Kersey, Berkoff and Morey 1st Euro Conf on Smart Structures and materials, Glasgow, 1992) Note that the detected signal shows the three reflected signal pulses from the three gratings. The amplitude of each of these three pulses varies slowly with time as the M-Z modulator is operated

Signal Returns from Backscatter Systems in Optical Fibre
(Return signal variation with time, for energy E, launched into the measurement fibre)

Conventional OTDR System:-

$$P(t) = P(z) = 0.5 \cdot E \cdot S \cdot \alpha_s(z) \cdot \exp\left[-\int_0^{z'} \alpha(z')dz'\right]$$

where (P(t) is the variation of return signal with time, P(z) is the equivalent variation with distance, z (z = v.t., where v is the velocity of light in fibre), S is the fraction of scattered light which is coupled into backward-guided modes in the fibre, $\alpha_s(z)$ is the scattering loss coefficient of the fibre, $\alpha(z)$ is the total attenuation coefficient of the fibre. The factor of 0.5 is included to allow for the 3dB loss for return light in the directional coupler.

Raman OTDR System:-

$$[P(t)]_{a-s} = [P(z)]_{a-s} = E \cdot S \cdot \eta_{a-s}\alpha(z) \cdot \exp\left[-\int_0^{z'} \alpha(z')dz'\right]$$

$$[P(t)]_s = [P(z)]_s = E \cdot S \cdot \eta_s \alpha(z) \cdot \exp\left[-\int_0^{z'} \alpha(z')dz'\right]$$

$$\text{Ratio, } R(t) = \eta_{a-s}/\eta_s = (\lambda_s/\lambda_{a-s})^4 \cdot \exp(-hcv/kT)$$

where η is the quantum efficiency of the Raman process in terms of the ratio of Raman scattered photons to attenuated photons, h is Plank's constant, c is the velocity of light in vacuo, k is the gas constant, λ is the wavelength of the Raman light and v is the frequency shift from the incident light wavelength. The subscripts a-s and s correspond to anti-Stokes and Stokes Raman light, respectively.

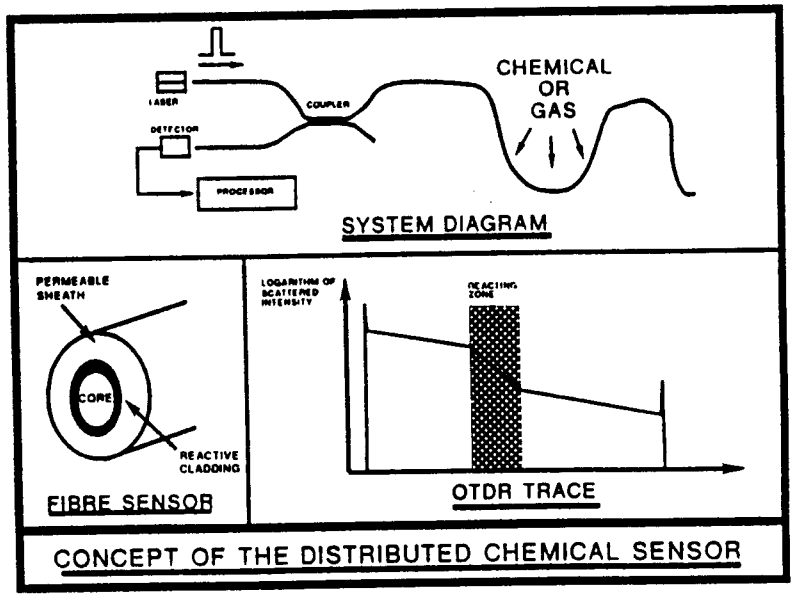

FLUORESCENT OTDR SYSTEMS

ADVANTAGES:-

- MUCH STRONGER SIGNAL RETURN THAN WITH NORMAL OTDR
- EASY TO SEPARATE SIGNALS IN TERMS OF BOTH TIME AND DIRECTION
- OUTGOING AND RETURN SIGNALS CAN SHARE A COMMON PATH
- LINEAR OPERATION, HENCE LESS CALIBRATION DIFFICULTY

DISADVANTAGES:-

- RELATIVELY LONG FLUORESCENT LIFETIMES OF VITREOUS DOPANTS LIMIT THE DISTANCE RESOLUTION TO SEVERAL TENS OF METRES.
- ATTENUATION IN THE FIBRE WILL GENERALLY PREVENT OPERATION OVER VERY LONG LENGTHS.
- SPECIAL FLUORESCENT FIBRE IS REQUIRED.

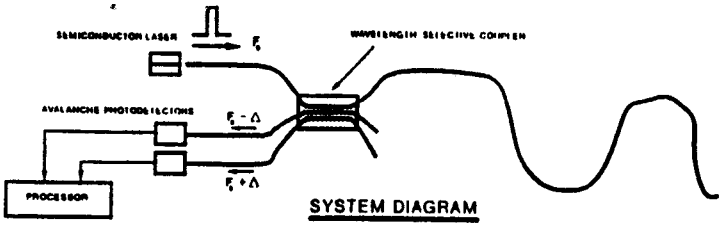

SYSTEM DIAGRAM

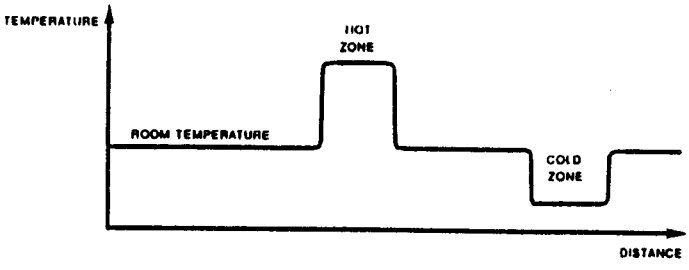

CONCEPT OF THE RAMAN DISTRIBUTED TEMPERATURE SENSOR

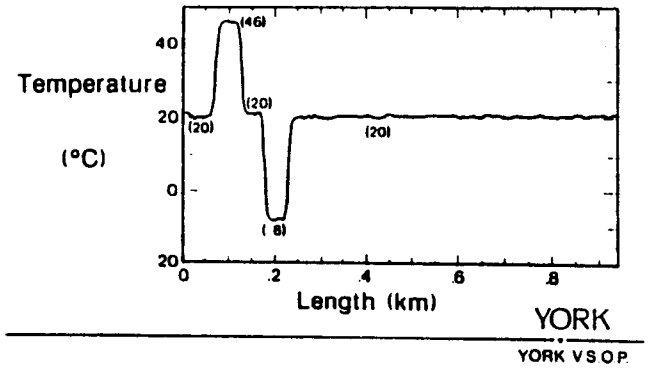

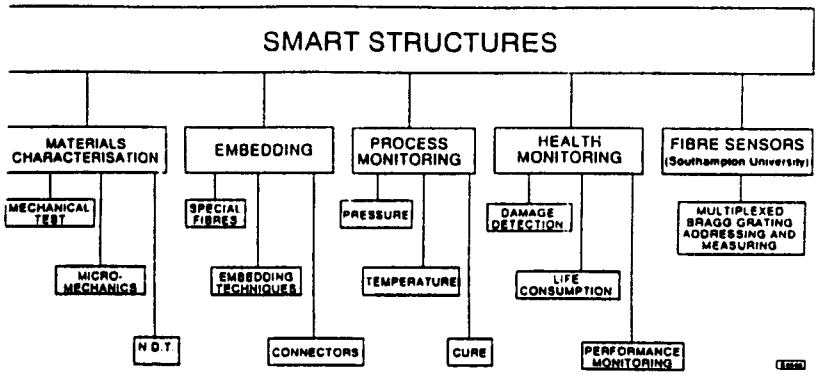

FIGURE 4 - SMART STRUCTURES RESEARCH ACTIVITIES

1. MECHANICAL TEST	· TENSION · COMPRESSION · INTER LAMINAR SHEAR · FATIGUE ASSESSMENT
2. NON-DESTRUCTIVE TEST	· ULTRASONIC "A" AND "C" SCAN · X-RAY - TRANSMISSION · X-RAY - BACK SCATTER AND TOMOGRAPHY
3. MICRO-MECHANICAL MODELLING	· STRESS FIELDS IN OPTICAL FIBRES · STRESS FIELDS IN HOST LAMINATES

FIGURE 6 - PROPOSED MATERIALS CHARACTERISATION PROGRAMME

TWIN-CORE FIBER OPTIC SENSOR

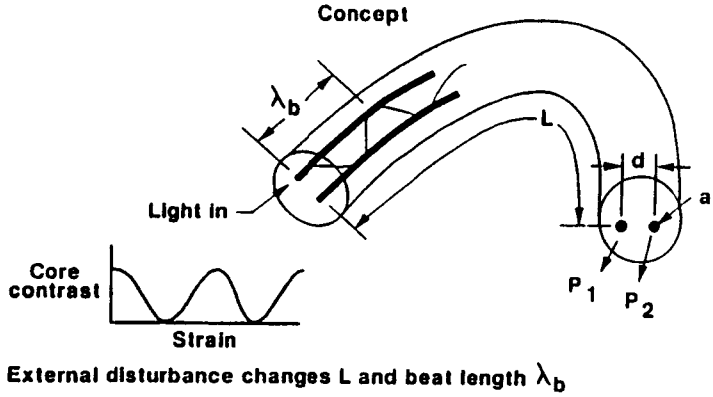

External disturbance changes L and beat length λ_b

Core contrast $(P_1 - P_2) / (P_1 + P_2)$ a function of $\phi = \pi (L / \lambda_b)$

WESTLAND AEROSPACE

DEMONSTRATOR PERFORMANCE

- Cantilever beam
- Step displacement disturbance

Passive System Response | **Active Damping System Response**

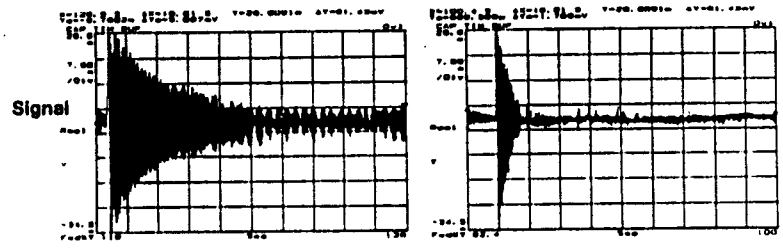

- 0.001 volt signal ≅ 0.001 inch deflection
- Resonant frequency ≅ 16.4 Hz
- Damping coefficient ≅ 2.5×10^{-3}
- Reduced vibrations
- Increased damping 7.3

WESTLAND AEROSPACE

TASK 2 - OUTPUT SENSOR SYSTEM

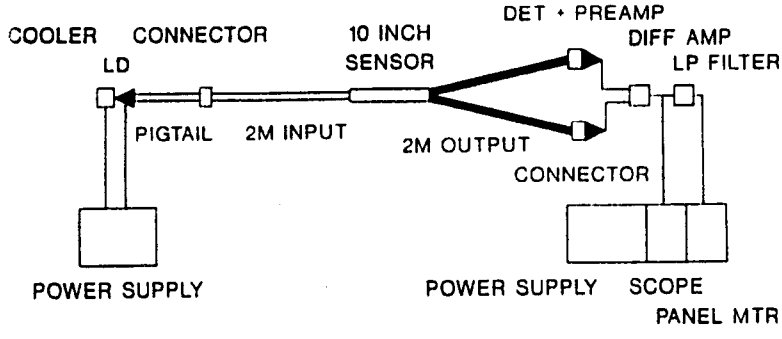

LASER DIODE 1 (STRAIN/VIB) - 830 nm
LASER DIODE 2 (TEMP) - nm

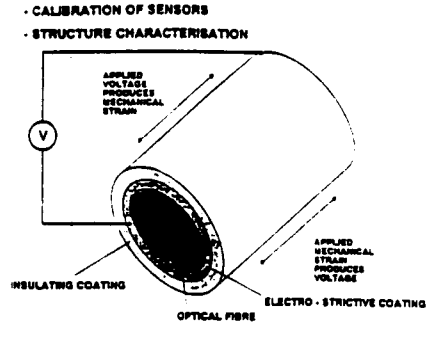

FIGURE 1a - INTEGRATED SENSOR/ACTUATOR PACKAGE

DAMAGE / DEFECT DETECTION - COMBINATION OF OPTICAL FIBRE SENSING AND ACTIVE FIBRE COATINGS PROVIDE MEANS FOR INTERROGATING MATERIAL AND STRUCTURE HEALTH

WESTLAND AEROSPACE

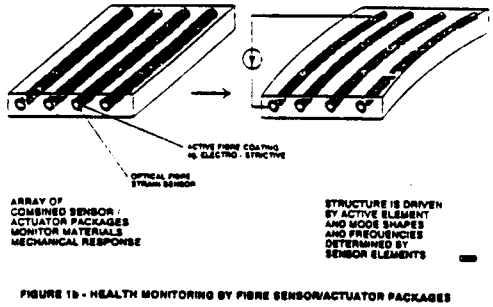

FIGURE 1b - HEALTH MONITORING BY FIBRE SENSOR/ACTUATOR PACKAGES

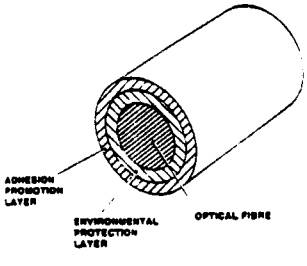

FIGURE 2 - GENERIC SENSOR/COATING PACKAGE

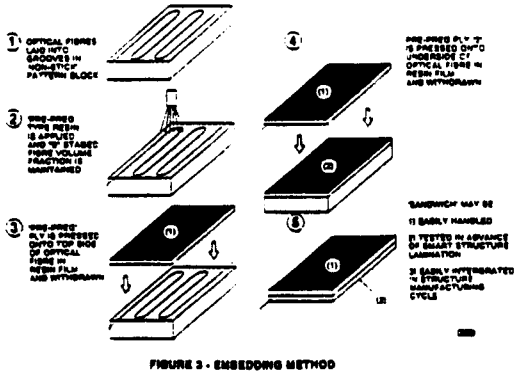

FIGURE 3 - EMBEDDING METHOD

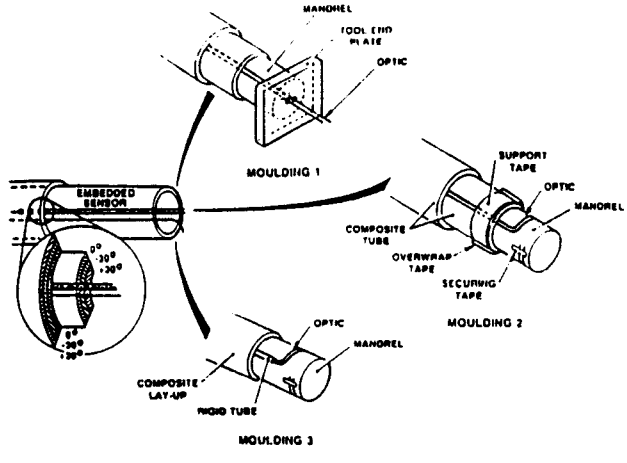

FIGURE 7 - SCHEMATIC OF THREE MOULDING APPROACHES

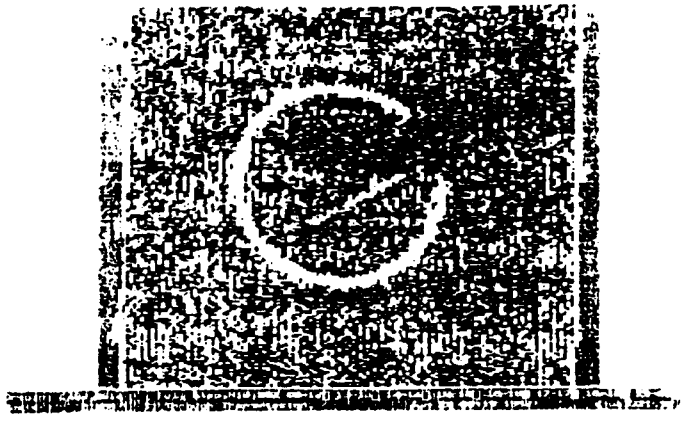

FIGURE 9 - 'C' SCAN INVESTIGATION - OPTICAL FIBRES IN GLASS PANEL

SOUTHAMPTON UNIVERSITY / EUROPEAN SPACE AGENCY PROGRAMME

SURFACE-MOUNTED FIBRE OPTIC SENSORS FOR COMPOSITE MATERIALS

OBJECTIVES:-

(i) To develop a multiplexed system to sense strain and temperature on the surface of composite space antennae

(ii) To derive surface deformations either from measurements of in-plane strain/temperature or from independent optical measurements